ACS OMEGA

Open Access

http://pubs.acs.org/journal/acsodf

Article

Silk Fibroin Nanoparticles as a Drug Delivery System of 3,3′-Diindolylmethane with Potential Antiobesogenic Activity

Calef Sánchez-Trasviña, Helen Y. Lorenzo-Anota, Aleyda M. Escobar-Fernández, David Lezama-Aguilar, Adriana Morales-Martínez, Ana Vélez-Barceló, Jorge Benavides, Omar Lozano, Marco Rito-Palomares, and Karla Mayolo-Deloisa*

Cite This: *ACS Omega* 2024, 9, 47661−47671

Read Online

ACCESS | Metrics & More | Article Recommendations | Supporting Information

ABSTRACT: Obesity is a global disease characterized by excessive lipid accumulation in the adipose tissue. There is an urgent need to explore alternative compounds to treat obesity. Low-molecular-weight compounds from plants, like 3,3′-diindolylmethane (DIM), are emerging as potential alternatives for obesity treatment. In this work, DIM is encapsulated into silk fibroin nanoparticles (SFNP) to evaluate the antiobesogenic potential. The obtained spherical-like SFNPs have a particle size between 165 and 200 nm, a polydispersity index between 0.11 and 0.15, and a zeta potential from −27 to −37 mV. DIM does not modify the nanoparticle shape but changes the secondary structure of fibroin and generates smaller nanoparticles (145 nm). DIM-loaded SFNP (SFNP-DIM) enhance their antioxidant capacity by 4.4-fold compared to SFNP. SFNP-DIM does not show cytotoxicity on white-like adipocytes, unlike 3T3-L1 preadipocytes, where cell viability decreased in a concentration-dependent manner. The SFNP-DIM treatment (5 μM, 0.03 mg SFNP mL^{-1}) does not modify the morphology of white-like adipocytes. It produces an apparent augmentation in the size and number of intracellular lipid droplets and increases by 2.18 ± 0.4-fold of triglyceride content. These findings demonstrated that SFNPs could be a potential delivery system of DIM, suggesting a potential therapeutic agent for treating obesity.

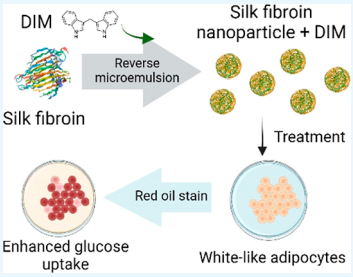

INTRODUCTION

Obesity is a global pandemic, increasing at alarming rates in adults, adolescents, and children.[1,2] In 2020, more than 2.6 billion people worldwide were diagnosed with obesity or being overweight, generating an economic impact of about US 1.96 trillion.[3] Unfortunately, the forecast is not encouraging; by 2030, half of the global population will be affected by obesity and obesity-related diseases, meaning an economic cost of about US 4.0 trillion.[3] Obesity is characterized by excessive lipid accumulation (triglycerides) in the adipose tissue due to several factors including an energetic imbalance between the intake and expenditure.[2] Obesity is considered a risk factor that predisposes children and adults to develop diseases such as metabolic syndrome, type 2 diabetes, insulin resistance, cardiovascular diseases, dyslipidemia, nonalcoholic fatty liver disease, COVID-19, renal disorders, and cancer.[2,4,5] Furthermore, obesity and its associated risks can decrease life expectancy from 5 to 20 years.[6] The treatment of obesity demands strategies that consider different approaches that including dietary restrictions, exercise, and pharmacotherapy.[7,8]

Nowadays, there are seven FDA-approved drugs for obesity treatment: setmelanotide, orlistat, liraglutide, semaglutide, phentermine-topiramate, naltrexone-bupropion, and tirzetapide.[1] Despite the positive results of antiobesogenic drugs, their use is limited by their significant side effects, such as cardiovascular and cerebrovascular problems, cancer, or psychological problems such as depression or suicidal ideation.[1,9] Therefore, developing novel treatments using molecules with fewer or null side effects is imperative. In this sense, many efforts have been focused on searching for novel natural molecules with antiobesogenic activities.[10,11] Low-molecular-weight molecules from plants, such as celastrol,[12] quercetin,[11] epigallocatechin 3-gallate,[11] and 3,3′-diindolylmethane (DIM), have been studied as antiobesogenic molecules, and results are promising.[13]

In the human body, DIM is formed by condensing two indole-3-carbinol molecules after ingesting cruciferous vegetables.[14] DIM has shown evidence of multiple therapeutic properties like antioxidant, anti-inflammatory, antiproliferative, and antitumor.[15] Furthermore, DIM demonstrated their potential to enhance the glucose uptake in adipocytes by overexpressing the glucose transporter 4 in adipocytes.[16] Additionally, it has been shown that DIM suppresses adipogenesis by inhibiting the ubiquitin-specific peptidase 2, but it also can inhibits high-fat diet-induced obesity in high-fat diet-fed obese mice.[13,16] Despite the tremendous therapeutic

Received: August 5, 2024
Revised: October 10, 2024
Accepted: November 8, 2024
Published: November 20, 2024

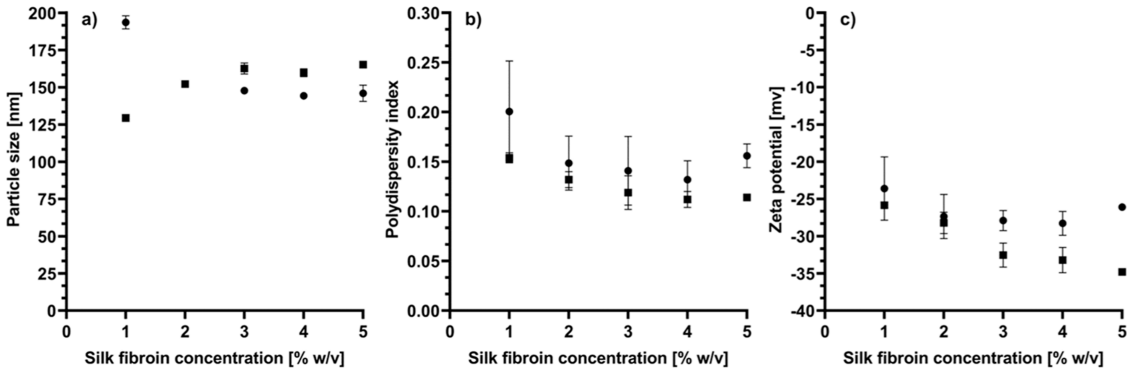

Figure 1. Solvent effect on SFNP synthesis. (a) particle size, (b) PDI, and (c) zeta potential. ● Ethanol ■ Acetone. All measurements were obtained by dynamic light scattering. Data are presented as a mean ± standard error (SE) of triplicates of at least three independent experiments.

potential of DIM, its physicochemical properties, like low solubility, high lipophilicity, and photosensitivity, reduce its bioavailability and restrict its use in pharmaceutical applications.[17,18] Therefore, drug carrier and delivery system strategies are needed to increase DIM bioavailability.

Nanoencapsulation is one of the most studied strategies to increase the bioavailability of low-soluble molecules, and it is considered a promising technique for obesity treatment.[19] Furthermore, different green processes have been developed for the production of nanosystems for drug carrier and delivery systems.[20] Several FDA-approved nanoencapsulated drugs are available on the market to treat diseases like leukemia, cancer, anemia, among others.[21] Some nanoencapsulation approaches have been studied to increase the bioavailability of DIM, including nanoparticles of primula oil and ethyl cellulose,[14] whey protein isolate,[17] and zein/carboxymethyl chitosan.[22] However, other biomaterials have a high potential for use as a nanoencapsulation material. In this context, fibroin, an FDA-approved biomaterial, is an emerging biopolymer being used for nanoencapsulation of proteins, nucleic acids, low-molecular-weight molecules, and antibiotics, among others.[23] Fibroin, commonly extracted from *Bombyx mori* silkworms, is a biodegradable, nontoxic, thermal stable, and biocompatible protein with desirable mechanical properties for fibers and nanoparticle synthesis.[24]

The present study aims to encapsulate DIM into SFNP for the first time. Different solvents (ethanol and acetone) and fibroin concentrations (1−5% w/v) were used to synthesize SFNP using the reverse microemulsion method, a strategy that has been poorly explored for SFNP synthesis. The effect of DIM encapsulation on the secondary structure of fibroin was analyzed and correlated with the size and zeta potential of nanoparticles. Furthermore, in vitro assays were performed to study the cytotoxicity of DIM-loaded nanoparticles on 3T3-L1 preadipocytes and white-like adipocytes. Lastly, the content of intracellular lipids was quantified to analyze the potential antiobesogenic activity of DIM-loaded SFNP.

■ RESULTS AND DISCUSSION

Particle Size, Polydispersity Index, and Surface Charge of SFNP. Silk fibroin nanoparticles (SFNPs) are a promising drug delivery strategy that improves the bioavailability of a broad range of molecules.[23] In this study, the reverse microemulsion method was used to synthesize SFNP, employing a commercial silk fibroin solution from *B. mori* silkworm, acetone, and ethanol as solvents, triton X-100 as a surfactant, and particles smaller than 200 nm were produced (see Figure 1a). It has been reported that protic solvents (ethanol), as well as aprotic solvents (acetone), can produce a conformational change of fibroin from the random coil and α-helix to β-sheet structures and allow the formation of particles of nanometric sizes.[25] The reverse microemulsion method has been poorly explored for the synthesis of SFNP despite a narrow particle size distribution that can be achieved.[26,27] Desolvation is one of the most used strategies to produce SFNP and several solvents like acetone, methanol, ethanol, isopropanol, and 1-propanol have been used.[25] Unlike desolvation, the reverse microemulsion method involves a surfactant to stabilize the micelles by reducing the surface tension.[27] Following this strategy, Myung et al. produced SFNP of 167 nm and polydispersity index (PDI) of 0.08 using triton X-100 as a surfactant and cyclohexane as a solvent.[28]

On the other hand, the effect of silk fibroin concentration on the synthesis of SFNP has been little studied. Therefore, in this work, different concentrations (1−5% w/v) were tested in both solvents using the reverse microemulsion method. It was observed that the raising of the silk fibroin concentration produced an opposite behavior when ethanol and acetone were used (see Figure 1a). Ethanol produces smaller particles when the fibroin concentration rises from 1 to 3% w/v; contrary, acetone produces larger particles when the fibroin concentration increases in the same range. The particle size remained constant for both solvents from 3 to 5% w/v of fibroin. When silk fibroin is in a solvent environment, it suffers an internal and external dehydration process and induces an alignment of hydrophobic regions that favors the formation of the crystalline form of Silk II and β-sheet structures.[27] The type of solvent affects the size and morphology of nanoparticles due to differences in the molecular structure, polarity, and hydrophilicity.[25,29] Those properties can affect the intermolecular interactions and produce differences in the nucleation rate of silk fibroin; a higher nucleation rate induces the formation of smaller particles.[29,30] In this context, at low fibroin concentrations, (1% w/v) the nucleation rate using acetone is higher than that of ethanol. However, the effect becomes the opposite when the fibroin concentration increases to 3% w/v. It has been reported that the fibroin concentration impacts the particle size of SFNP.[31] Typically, it is expected that the particle size increases when the protein concentration also increases due to an increase in particle collision, which leads to agglomeration.[29] This effect is even observed when SFNP are obtained by the salting-out method.[31] In this work, SFNP produced by reverse microemulsion using acetone follow this phenomenon; however, smaller nanoparticles are obtained at

https://doi.org/10.1021/acsomega.4c07203
ACS Omega 2024, 9, 47661−47671

higher fibroin concentrations when ethanol is used. This behavior was reported previously by Lin et al., where SFNP were produced using ethanol and the desolvation method. They obtained SFNP of 359 nm using 0.5% w/v of fibroin solution, but the size was reduced to 293 nm when 3.5% w/v of fibroin solution was used.[32]

The particle size distribution was determined by dynamic light scattering (DLS). Figure 1b shows the effect of the type of solvent and fibroin concentration on the PDI of SFNP. For both solvents, higher fibroin concentrations favor the production of SFNP with a narrow particle size distribution (from 0.21 to 0.12). In general terms, PDI values below 0.3 are considered acceptable for nanoparticles to be used in biotechnological applications.[32] In counterpart, higher PDI values could affect the surface area of nanoparticles available for adsorption, reduce the capability of drug loading of a particular part of the nanoparticle population, and in consequence, irregular pharmacokinetics could be obtained.[33] From Figure 1b, it can be seen that acetone produces more uniform particle sizes than ethanol. This effect has been observed previously.[25] PDI values obtained in this work are higher than those obtained by Myung et al. (0.08) using the reverse microemulsion method but employing cyclohexane as a solvent, which could induce different nucleation rates and intermolecular interactions favoring lower PDI.[28,29] However, in comparison to SFNP produced by desolvation using the same solvents, the PDI values in this work are in the same range (from 0.109 to 0.327).[32,34]

Lastly, Figure 1c shows the effect of fibroin concentration and solvent type on SFNP zeta potential. Both solvents produced SFNP with a negative surface charge between −22 and −35 mV. When ethanol is used, and the fibroin concentration rises, the zeta potential is maintained in the range between −22 and −25 mV. In contrast, acetone reduced the surface charge from −26 to −35 mV when the fibroin concentration increased. The negative surface charge is a characteristic of SFNP, ranging between −10 and −31 mV with organic solvents,[32,35] or even up to −46 mV when the salting-out method is used.[31] It has been reported that more than half of the ε-amino groups are on the surface of the SFNP produced with organic solvents.[25] The N-terminal residue of fibroin has a negative net charge (pI 4.6), and the hydrophobic repetitive domains of fibroin structure, which possess a hydrophilic spacer, also have a negative charge (pI 3.8). Therefore, it is expected to obtain SFNP with a negative zeta potential.[31] An increase in zeta potential is associated with more compact structures due to less electrostatic repulsion. In counterpart, a more negative surface charge is related to less dense and larger particles but is more stable due to additional hydrophobic interactions.[31] Therefore, the nature of both solvents (ethanol and acetone) and fibroin concentration could induce a different structural conformation of fibroin, altering the electrostatic and hydrophobic interactions. In consequence, the surface charge of the nanoparticles will depend on the solvent and the fibroin concentration. Because a higher fibroin concentration produces more stable SFNP than the low fibroin concentration, SFNP produced with 5% w/v of fibroin using acetone and ethanol were selected for further experiments.

Morphology and Secondary Structure of SFNP. The morphology of SFNP was analyzed by scanning electron microscopy (SEM), as shown in Figure 2. Both solvents produced spherical-like nanoparticles. However, different behaviors were observed. SFNP produced by acetone showed

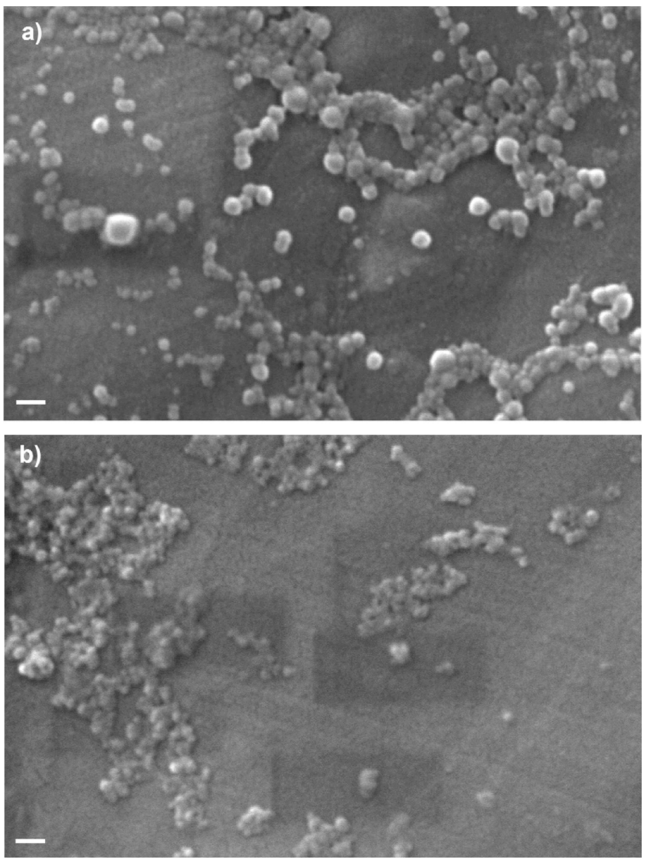

Figure 2. SEM micrographs of SFNP using (a) acetone or (b) ethanol as a solvent. All nanoparticles were prepared by the reverse microemulsion method using 5% w/v of silk fibroin solution. Scale bar 200 nm.

a low tendency to aggregation (Figure 2a) compared to those produced by ethanol, which were aggregated (Figure 2b). A similar aggregation of SFNP, produced by the salting-out method, was observed by SEM previously.[31] It has been reported that SFNP produced with ethanol and methanol by the desolvation method can be easily aggregated; meanwhile, acetone does not induce this phenomenon.[25] Regarding the particle size, SEM images revealed that SFNP produced by acetone (Figure 2a) are larger than those produced by ethanol (Figure 2b), which agrees with data from DLS analysis. In both cases, the sizes observed in SEM images are smaller than those obtained by DLS because DLS measures the hydrodynamic diameter.[33]

Because those SFNP produced by acetone and using the 5% w/v fibroin concentration showed spherical-like particles with excellent stability according to DLS analysis, these particles were lyophilized and further analyzed by FTIR. Figure 3a shows FTIR spectra of SFNP (blue line), and characteristic bands of fibroin were observed: C−N stretch of amide III (1230−1270 cm^{-1}), N−H bend of amide II (1520−1540 cm^{-1}), and C═O stretch amide I (1610−1650 cm^{-1}).[36] Furthermore, in the band of amide I (Figure 3b), a peak is observed at 1622 cm^{-1} corresponding to silk II, which is characterized by β-sheet structures present in SFNP.[31] For further information, a deconvolution of the amide I region was performed. Amide I band is the most used infrared band for determining the secondary structure of proteins. In this band, structures like α-helices, β-sheets, β-turns, random coils, and

https://doi.org/10.1021/acsomega.4c07203
ACS Omega 2024, 9, 47661−47671

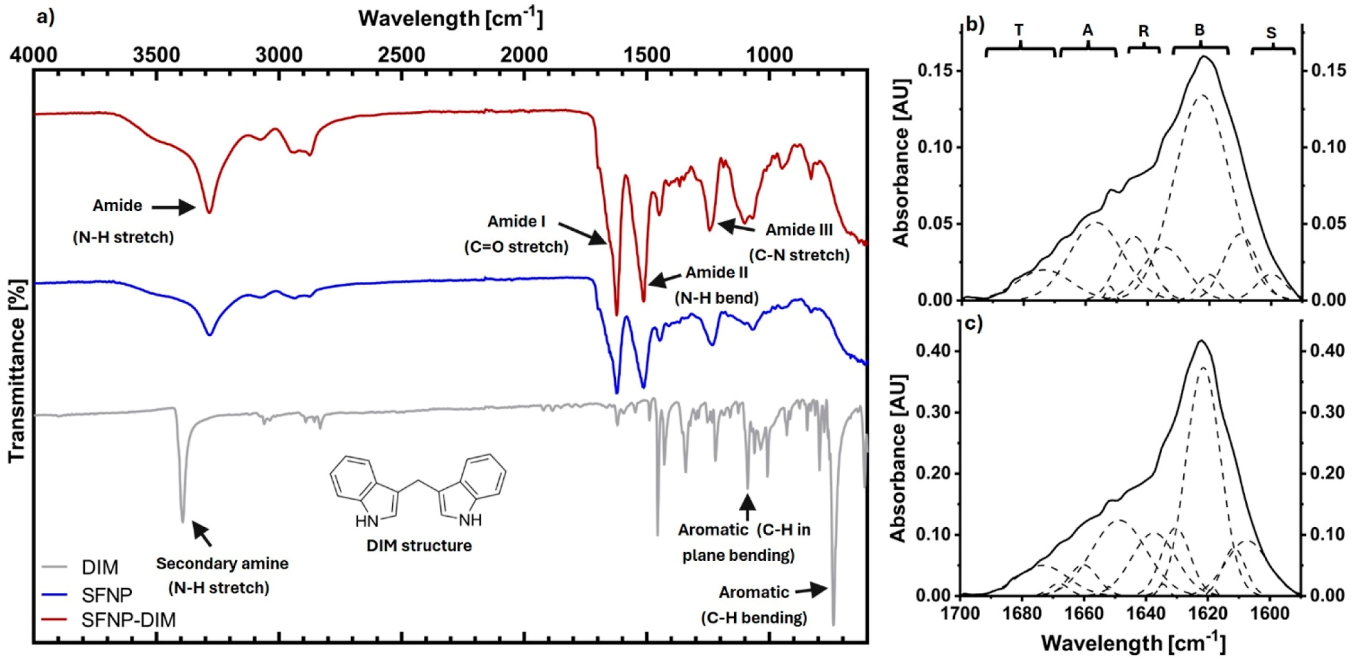

Figure 3. Structural analysis of SFNP. (a) FTIR spectrum of DIM, SFNP, and SFNP loaded with DIM (SFNP-DIM); (b) deconvolution of amide I (1590−1700 cm^{-1}) of SFNP; and (c) deconvolution of amide I (1590−1700 cm^{-1}) of SFNP-DIM. All SFNP were produced using acetone as the solvent and fibroin concentration of 5% w/v. Secondary structures identified by β-turns (T), α-helix (A), random coil (R), inter- and intramolecular β-sheets (B), and side chains (S).

side chains can be identified by deconvolution.[31,37] SFNP produced by reverse microemulsion, using acetone and 5% w/v of fibroin concentration, are composed mainly by β-sheets (55.7%) followed by random coils (18.1%), α-helix (16.7%), β-turns (6.5%), and side chains (3.0%). When fibroin forms nanoparticles, the β-sheet is the most abundant secondary structure.[31,38] SFNP produced by the salting-out method can reach 39.4% of β-sheet structures.[31] Meanwhile, SFNP produced by nanoprecipitation using a mixture of acetone-ethanol reached 35.3%.[38] Also, SFNP produced by nanoprecipitation using isopropanol showed a similar overall secondary structure composition obtained in this work.[39]

DIM Encapsulation into SFNP. Natural molecules have been explored as alternatives to antiobesogenic treatments. DIM has been demonstrated as a potential drug against obesity; however, its low bioavailability restricts its application in further studies.[17,18] Therefore, DIM was encapsulated into SFNP to improve its bioavailability and enhance its biological activity. Due to the stability of the nanoparticles, SFNP produced with 5% w/v of fibroin solution and acetone were used for the DIM encapsulation. Different DIM-fibroin mass ratios were used, and Table 1 shows the results. The particle size of SFNP loaded with DIM (SFNP-DIM) was smaller than that of SFNP without DIM; meanwhile, the PDI remained similar. For its part, the zeta potential of SFNP-DIM increased slightly compared to SFNP. The DIM molecule is highly hydrophobic; therefore, its presence when SFNPs are forming affects the structural conformational change of fibroin. The DIM could interact with the hydrophobic domains (Gly-Ala-Gly-Ala-Gly-Ser) of the heavy chain of fibroin, and as a result, the nanoparticles are more compact.[23] Besides, these structural changes reduce the ε-amino groups exposed on the surface of SFNP, and consequently, the surface charge of SFNP-DIM becomes more positive. So far, there are no reports about DIM encapsulation in SFNPs; however, other proteins have been tested. Khan et al. produced DIM-loaded nanoparticles of whey protein isolate, and they observed different behaviors. In their work, DIM increased the nanoparticle's size from 100 to 150 nm, decreased the zeta potential from −30 to −50 mV, and maintained a similar PDI.[17]

Table 1. Effect of DIM Encapsulation on SFNP[a]

DIM/fibroin mass ratio	DIM loading capacity (%)	size [nm]	PDI	zeta potential [mv]
		165 ± 2	0.11 ± 0.01	−37.7 ± 2.5
1:40	0.1 ± 0.04	146 ± 6	0.13 ± 0.01	−35.0 ± 1.3
1:20	0.2 ± 0.02	184 ± 4	0.19 ± 0.01	−35.6 ± 1.8
1:10	0.6 ± 0.54	150 ± 2	0.15 ± 0.01	−31.4 ± 0.9
1:2.5	0.5 ± 0.60	131 ± 1	0.13 ± 0.01	−33.4 ± 0.8
1:1	4.6 ± 1.10	145 ± 6	0.12 ± 0.00	−30.9 ± 0.6

[a]All nanoparticles were prepared using 5% w/v of silk fibroin solution and acetone as a solvent. Data are presented as a mean ± SE of triplicates of at least three independent experiments.

Regarding the drug loading content of SFNP-DIM, the DIM-fibroin mass ratio has a significant effect on the loading efficiency (see Table 1). When the DIM/fibroin mass ratio decreases, it is possible to encapsulate more DIM. This effect was opposite when Khan et al. encapsulated DIM in whey protein isolate nanoparticles due to the difference in the type of proteins and the nanoparticle preparation method.[17] In their work, Khan et al. obtained DIM encapsulation efficiencies between 80 and 90% (drug loading content was not reported). However, the PDI of nanoparticles were ≥0.3, which could compromise its pharmacokinetic reproducibility. On the other hand, Mattiazzi et al., who encapsulated DIM using Eudragit RS100 or ethyl cellulose as a shell and different oils as the core, reached a drug loading of 950−970 μg DIM mL^{-1}, a value much higher than that obtained in this work (46 μg DIM mL^{-1}).[14] However, their nanoparticles possess a zeta potential close to neutrality (−13 to 12 mV) compromising the

https://doi.org/10.1021/acsomega.4c07203
ACS Omega 2024, 9, 47661−47671

nanoparticle stability. Therefore, despite the low DIM loading in SFNP, the DIM encapsulation in SFNP presents advantages over previous DIM encapsulation approaches due to the high stability, narrow particle distribution, and synthesis reproducibility of SFNP. Besides, SFNP-DIM showed in vitro activity as it will be shown in the next sections.

To corroborate and understand the conformational changes produced by DIM, DIM and SFNP-DIM were analyzed by Attenuated total reflection Fourier transform infrared spectroscopy (ATR−FTIR) (see Figure 3a). DIM IR spectrum has different representative bands (Figure 3a, gray line): 3400 cm^{-1} (N−H stretch of the secondary amine), 1450 cm^{-1} (C−C stretch of aromatic), 1080 cm^{-1} (C−H in-plane bending), and 735 cm^{-1} (C−H out of plane bending).[40] In comparison to SFNP, SFNP-DIM showed several differences along all spectra. The bands of fibroin nanoparticles like amide III (1230−1270 cm^{-1}), amide II (1520−1540 cm^{-1}), and amide I (1610−1650 cm^{-1}) were visualized with no wavelength shift.[36] However, the intensity of all amide bands is different, which indicates the addition of the N−H group of DIM and the exposure of amino acid residues.[41] The C−N, C═O, and N−H groups are involved in the formation of hydrogen bonds. Therefore, the intensity change of amide bands can be attributed to hydrogen bonds between DIM and SFNP. Additionally, the C−H antisymmetric stretch bands (2800−3000 cm^{-1}) are related to hydrophobic interaction;[41] therefore, changes in the intensity of those bands revealed that DIM is also interacting with SFNP by hydrophobic interactions.

The amide I region's intensity change revealed that the secondary structure was modified. Therefore, the amide I band was deconvoluted for further analysis. The encapsulation of DIM into SFNP produced changes in the secondary structure in comparison with SFNP (Figure 3c): β-sheet content decreased from 55.7 to 47.5%, α-helix increased from 16.7 to 22.0%, random coils decreased from 18.1 to 12.6%, side chains, and β-turns increased from 3.0 to 10.1% and 6.5 to 7.8%, respectively. The heavy chain of silk fibroin possesses 12 hydrophobic domains in tandem with 11 hydrophilic domains, with repetitive sequences of Gly-Ala-Gly-Ala-Gly-Ser. When the nanoparticles form, those domains interact through intra- and interhydrogen bonds and van Deer Wals forces to produce β-sheet structures.[23] The DIM molecule interacts with SFNP by hydrogen bonds and hydrophobic interactions. Therefore, when the nanoparticle forms, DIM alters the formation of hydrogen bonds between the hydrophobic domains of fibroin heavy chain and modifies the secondary structure of SFNP.

Lastly, the morphology of SFNP-DIM was analyzed by SEM (Figure 4). It was observed that SFNP-DIM has a spherical-like shape but a smaller particle size than SFNP. This observation agrees with the data from Table 1, where the particle size decreases with the presence of DIM. Furthermore, it was observed that SFNP-DIM are more aggregate than SFNP (Figure 2a). This aggregation is correlated with the rise of the zeta potential of SFNP-DIM, attributed to the change of the secondary structure of fibroin, which could promote more interactions between nanoparticles and form aggregates.

Antioxidant Capacity of SFNP-DIM. It has been demonstrated that DIM possesses antioxidant properties.[15,17] Therefore, the ABTS scavenging capacity of SFNP-DIM was assessed. Figure 5 shows the antioxidant capacity of DIM at different concentrations. The antioxidant capacity is attributed to the two N−H groups in its structure, which can donate −H groups and neutralize free radicals.[15] SFNP produced by

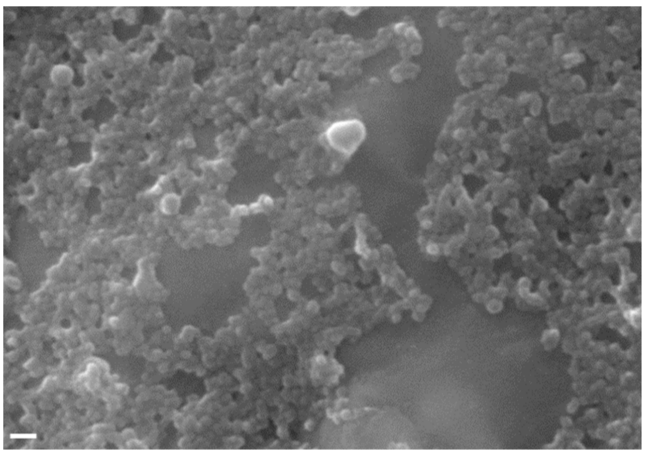

Figure 4. SEM micrographs of SFNP loaded with DIM. Nanoparticles were prepared by the reverse microemulsion method using 5% w/v of silk fibroin solution at DIM/fibroin mass ratio 1:1. Scale bar 200 nm.

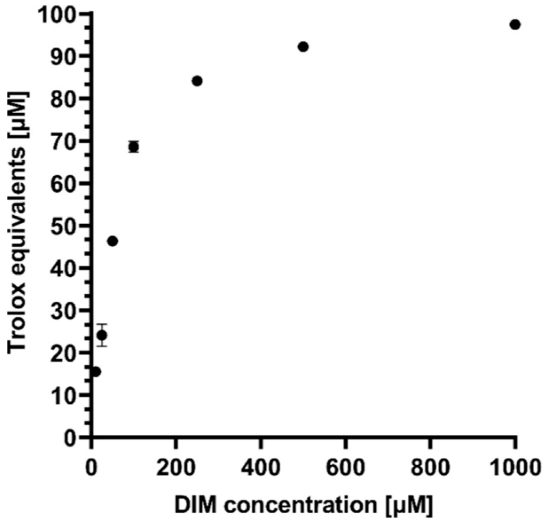

Figure 5. Antioxidant capacity of DIM based on the discoloration of the ABTS radical cation after its reduction to ABTS. Data are presented as a mean ± SE of triplicates of at least three independent experiments.

reverse microemulsion, using 5% w/v of fibroin solution and acetone, showed an antioxidant capacity of 10.74 ± 0.27 μM Trolox equivalents. However, when DIM was encapsulated into SFNP, the antioxidant capacity increased to 47.13 ± 1.45 μM Trolox equivalents. It has been reported that SFNP, produced by desolvation using acetone as a solvent, increased the antioxidant capacity of RAW 264.7 cells when treated with 0.1 mg SFNP mL^{-1}.[42] The antioxidant capacity of SFNP is attributed to the presence of hydroxyl, carboxyl, and amine groups of all amino acid residues.[43] In order to analyze the encapsulation effect, the DIM concentration in the SFNP-DIM solution was calculated based on the drug loading. The obtained DIM concentration (183 μM) corresponds, according to Figure 5, to 77 μM Trolox equivalents, which is 2-fold of the antioxidant capacity of SFNP-DIM. This reduction of the antioxidant capacity is opposite to the previous report where DIM was encapsulated in Eudragit RS100 and ethyl cellulose nanoparticles.[15] This different behavior can be attributed to the difference in the nanoparticles materials and the synthesis process. Because DIM is encapsulated during the nanoparticle

https://doi.org/10.1021/acsomega.4c07203
ACS Omega 2024, 9, 47661−47671

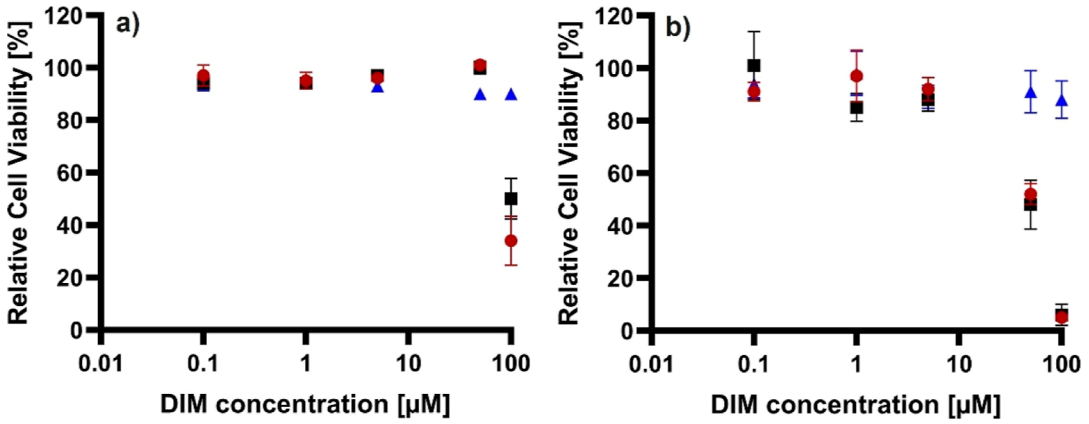

Figure 6. Cytotoxic effect of DIM, SFNP, and SFNP-DIM on (a) white-like adipocytes and (b) 3T3-L1 preadipocytes. Relative cell viability analysis quantification was done by Alamar blue using different concentrations 0.1, 1, 5, 50, and 100 μM of DIM, SFNP, and SFNP-DIM during 24 h. ● SFNP-DIM, ■ SFNP, ▲ DIM. The equivalent concentration of SFNP-DIM was determined based on DIM drug loading. Data are presented as a mean ± SE of triplicates of at least three independent experiments.

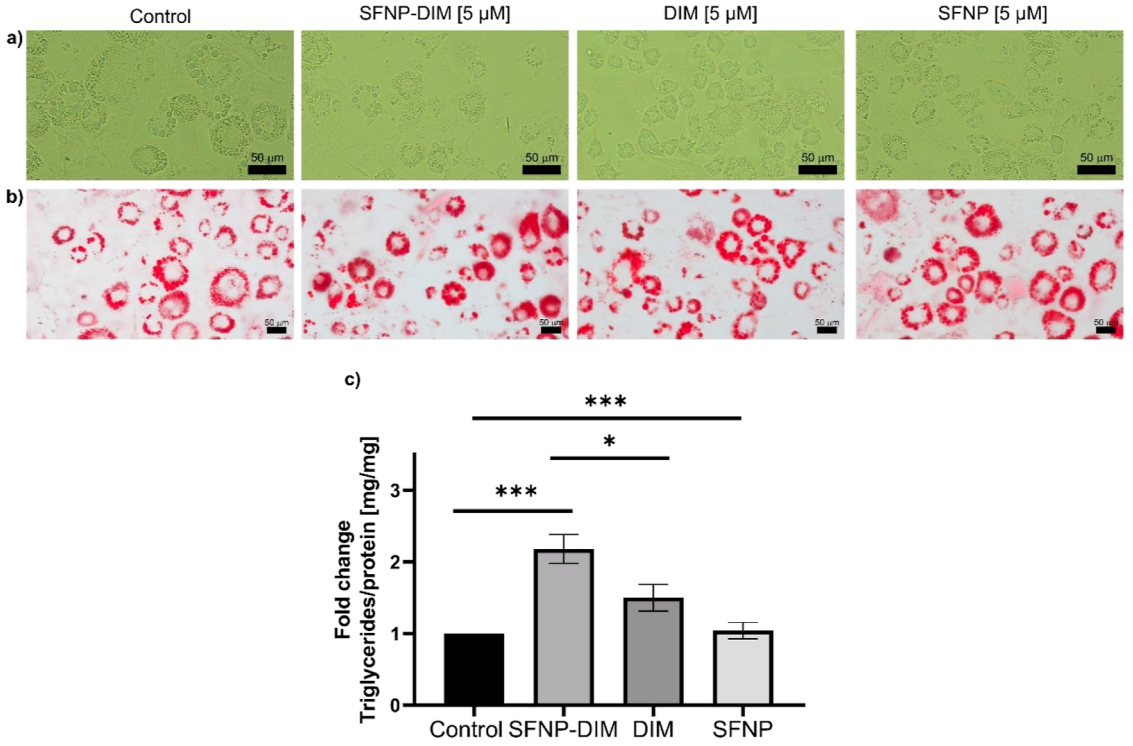

Figure 7. Morphology of (a) white-like adipocytes at 10 days of differentiation, (b) oil red staining of white-like adipocytes at 10 days of differentiation, and (c) triglycerides quantification of white-like adipocytes at 10 days of differentiation treated with 5 μM of DIM, SFNP, and SFNP-DIM. The equivalent concentration of SFNP-DIM was determined based on DIM drug loading. Scale bar 50 μm. Data are presented as a mean ± SE of triplicates of at least three independent experiments. *p < 0.05, ***p < 0.001.

synthesis, where fibroin changes its structure, DIM could be entrapped in the fibroin structure and can be less accessible to the ABTS radical. However, despite the reduction of antioxidant capacity, in comparison to free DIM, the DIM encapsulation in SFNP extends the antioxidant capacity over time. After six months, the SFNP-DIM showed 13.7 ± 1.1 μM Trolox equivalents (29 ± 2.3% of the initial antioxidant capacity); meanwhile, SFNP did not show antioxidant capacity.

Cytotoxic Effect of SFNP-DIM on 3T3-L1 Preadipocytes and White-Like Adipocytes. Before analyzing the potential antiadipogenic effect of SFNP-DIM, a cytotoxicity assay was performed at 24 h of treatment on white-like adipocytes differentiated until day 10. Because SFNP has not been tested on white-like adipocytes, a wide range of concentrations were tested from 0.52 μg/mL to 0.52 mg/mL, equivalent to 0.1−100 μM of DIM. Figure 6a exhibits that DIM does not affect cell viability on white-like adipocytes even at 100 μM; however, at the same concentration, SFNP and SFNP-DIM (0.52 mg SFNP mL^{-1}) decreased cell viability at 50 and 34%, respectively. Then, the cytotoxicity on the lineage precursor 3T3-L1 preadipocytes was assessed. Figure 6b shows that DIM does not show cytotoxicity on 3T3-L1 preadipocytes even at 100 μM. However, SFNP and SFNP-DIM decreased around 50% of relative cell viability at 50 μM (0.26 mg SFNP mL^{-1}) and around 100% at 100 μM (0.52 mg SFNP mL^{-1}).

https://doi.org/10.1021/acsomega.4c07203
ACS Omega 2024, 9, 47661−47671

Interestingly, no affections were observed at low SFNP and SFNP-DIM concentrations (0.1−5 μM). These results demonstrate that DIM does not have cytotoxicity upon adipocytes and 3T3-L1 preadipocytes, contrary to SFNP and SFNP-DIM, which suggest SFNP brings cytotoxicity. The cytotoxicity of SFNP has been studied in different cell lines; nonetheless, to our knowledge, this is the first time white-like adipocytes and 3T3-L1 preadipocytes have been tested. When SFNPs were tested with tumor cell lines (Caco-2, HepG2, and 9L), no cytotoxicity effect was observed even at 1 mg SFNP mL^{-1}.[44] Nevertheless, when fibroblast, Huvec, and RAW 264.7 cells were treated with SFNP, their viability was reduced by approximately 50% using 0.5 mg SFNP mL^{-1}.[42,45] It was reported that SFNPs could upregulate the expression of colony-stimulating factors, chemokines, proinflammatory cytokines, and TNF-α in macrophages.[42] Additionally, hydrolysate silk fibroin has been reported to reduce the viability of 3T3-L1 preadipocytes below 80% at 24 h and 0.1 mg mL^{-1}.[46] The results suggest that SFNP, and in consequence, SFNP-DIM, could induce apoptosis on adipose tissue-derived cells. Hence, 5 μM DIM equivalent to 0.03 mg SFNP mL^{-1} (concentration where cell viability was reduced less than 10%) was used for further experiments.

Effect of SFNP-DIM on Intracellular Triglycerides in White-Like Adipocytes. Adipogenesis is a mechanism where preadipocytes become adipocytes through differentiation that accumulates triglycerides into lipid droplets, which could provoke adipocyte hypertrophy, leading to obesity-related disorders.[47] Recently, it has been demonstrated that adipogenesis prevents obesity-mediated metabolic decline.[48] Therefore, one novel opportunity to control or manage obesity is through controlling adipogenesis through naturally derived compounds such as DIM. Thus, once the cytotoxicity of SFNP-DIM was determined, it was decided to analyze if the encapsulation of DIM into SFNP could modify the antiadipogenic effect of DIM on 3T3-L1 preadipocytes. In this sense, 3T3-L1 preadipocytes were stimulated with 5 or 50 μM of DIM, SFNP-DIM, or SFNP during the differentiation's stimulus until day 10. The untreated cells (control group) showed abundant intracellular lipid droplets (Figure 7a), which is a typical morphology of adipocytes.[49] Interestingly, the groups stimulated with 5 μM SFNP-DIM or free DIM did not show substantial morphological changes compared to the control. At the same dose, SFNP exhibited a similar morphology (Figure 7a). Cells stimulated with 50 μM of DIM did not show morphological alterations compared to untreated cells. In contrast, when the cells were stimulated with 50 μM SFNP or SFNP-DIM (0.52 mg SFNP mL^{-1}), few attached cells were observed, which did not show a classical adipocyte morphology (Figure S1a). These results, considering the cell viability (Figure 6b) on 3T3-L1 preadipocytes, suggest that 50 μM SFNP or SFNP-DIM reduce the cell viability and, consequently, the adipocyte differentiation process is compromised. Then, the intracellular lipid content was analyzed using oil red staining. SFNP-DIM (5 μM) increased intracellular lipid droplet accumulation (an apparent augmentation in the size and number) compared to the control, and with free DIM (5 μM), SFNP did not show an apparent change (Figure 7b). Contrarily, at 50 μM of SFNP-DIM or SFNP, which compared to control, several fragments of nanoparticles were observed. Interestingly, DIM apparently increased intracellular lipid content in size and number compared to the control (Figure S1b). The augmentation of intracellular lipid droplets in the size and number is associated with significant adipocyte proliferation or differentiation.[50] Also, lipid metabolism is modulated by adipogenesis and lipolysis and orchestrated by several enzymes that regulate the adipocyte phenotype.[51]

Finally, the intracellular triglycerides were quantified to confirm the antiadipogenic effect of SFNP-DIM. SFNP-DIM (5 μM) significantly increased triglyceride content (2.18-fold) compared to the control, DIM, and SFNP treatment (Figure 7c). Additionally, the triglyceride content was reduced on cells stimulated with SFNP-DIM and SFNP 50 μM, attributed to the cell viability reduction; meanwhile, DIM at 50 μM significantly increases triglyceride content (Figure S1c). Together, these results demonstrated that low SFNP-DIM concentration (5 μM) enhances the capability of free DIM to accumulate triglycerides into adipocytes while having a contrary effect at 50 μM. The reported effect of DIM is controversial; some studies demonstrated that at high doses prevents adipogenesis through the AMPKα-pathway and by inhibiting the ubiquitin-specific peptidase 2.[13,52] Other authors reported that low DIM concentrations (5 μM) increase insulin sensitivity by high glucose uptake, provoking lipid augmentation in adipocytes.[16] A similar controversy was reported on silk fibroin, on the one hand, it inhibits adipocyte differentiation but promotes browning in the white adipose tissue by suppressing adipogenesis through the AMP-activating protein kinase and uncoupling protein-1 (UCP-1) pathway.[46,53] On the other hand, another research group demonstrated that silk fibroin inhibits lipid accumulation, decreasing adipocyte differentiation, downregulating genes associated with adipogenesis such as PPARγ and C/EBPα, and upregulating UCP-1 and CPT-1.[46]

Based on the controversial previous reports, it is hypothesized that SFNP-DIM could exert two or more different mechanisms over white-like adipocytes. At low DIM-SFNP concentration (5 μM), it is enhanced the capability of free DIM to accumulate triglycerides. This suggests the promotion of adipogenesis by increasing the glucose uptake on adipocytes. Contrary, 50 μM of SFNP-DIM on 3T3-L1 preadipocytes reduces the cell viability, suggesting the possibility of acting as an apoptotic inductor or proliferator inhibitor. In general, the evidence demonstrated the application of SFNP to potentiate the effect of DIM at low concentrations.

CONCLUSIONS

This work shows an alternative strategy for DIM encapsulation in SFNP. The reverse microemulsion method, using acetone and ethanol as solvents, allows the production of SFNP with particle size <200 nm, narrow polydispersity (PDI < 0.2), and highly stable (ZP < −24 mV). The type of solvent affects the nucleation rate of nanoparticles and, consequently, the particle size. Moreover, the solvent affects the conformational change of fibroin during the nanoparticle formation. Particularly, when acetone is used, spherical-like SFNPs are more stable than with ethanol. The predominant secondary structure of fibroin, when forming SFNP, is the β-sheet (55.7%). However, the DIM encapsulation induces conformational changes that modify the secondary structure of fibroin when the SFNP form and reduces the particle size. When DIM is encapsulated in SFNPs, it interacts with fibroin molecules through hydrogen bonds and hydrophobic interactions. Furthermore, DIM showed a synergistic antioxidant effect when was encapsulated in SFNPs, which could be prolonged during the time due to

https://doi.org/10.1021/acsomega.4c07203
ACS Omega 2024, 9, 47661−47671

the encapsulation process. SFNP-DIM at 50 μM DIM ($\leq$0.26 mg SFNP mL^{-1}) does not produce significant cytotoxicity upon white-like adipocytes; however, on preadipocytes 3T3-L1, cell viability is affected in a concentration-dependent manner at 24 h. The cytotoxic effect of SFNP could be addressed by chemical modifications on the surface of nanoparticles or by increasing the drug loading content. On the other hand, during adipogenesis at 5 μM (0.03 mg SFNP mL^{-1}), SFNP-DIM does not produce morphological changes on white-like adipocytes but exhibits an apparent augmentation on intracellular lipid droplets (size and number). In addition, SFNP-DIM increases the triglyceride content in white-like adipocytes. These findings confirm that SFNP is a potential drug delivery system for molecules such as DIM for treating obesity-associated disorders. Moreover, further metabolic analysis in vitro and in vivo of obesity-related markers, gene expression, and anthropometric measurements will provide more detailed information about the antiobesogenic effect.

It can be concluded that this study provides new methodologies to produce SFNP which can be used for the encapsulation of molecules with biomedical applications. Moreover, the capability of SFNP to be used as a drug carrier system for antiobesogenic treatment may be extrapolated to other active agents besides DIM, increasing the bioavailability and overall efficiency of the obesity treatment.

METHODS

Silk fibroin from *B. mori* silkworm, triton X-100, 2,2′-azinobis(3- ethylbenzothiazoline-6-sulfonic acid) diammonium salt (ABTS), 6-hydroxy-2,5,7,8-tetramethylchromane-2-carboxylic acid (Trolox), ethanol HPLC grade, and DIM were acquired from Sigma-Aldrich (St. Louis, MO, USA). Methanol and acetone were purchased from J.T. Baker (Center Valley, PA, USA). Acetonitrile (ACN) was acquired from Honeywell (Charlotte, CA, USA). All experiments were done using HPLC water.

SFNP Synthesis. The SFNPs were prepared following the method reported by Myung et al.[28] with modifications. Briefly, 785 μL of either ethanol or acetone were mixed with 185.2 mg of triton X-100, and then 42 μL of silk fibroin solution at different concentrations (1−5% w/v) was added. The mixture was mixed by vortex for 1 min and then centrifugated at 14,000 rpm, 30 min at 4 °C (Microfuge 22R, Beckman Coulter, CA, USA). The supernatant was discarded, the pellet was washed three times with water, reaching a final volume of 2 mL. The particles were sonicated with a 1/8″ probe using a Q125 Sonicador (Qsonica, Newtown, USA) 1 min ON/OFF cycle for 20 min and 20% amplitude in an ice bath. Unless otherwise mentioned, the final suspension was kept in water at 4 °C for further analysis.

DIM Encapsulation. For the DIM encapsulation, different DIM/fibroin mass ratios were used (1:40, 1:20, 1:10, 1:2.5, and 1:1). DIM was dissolved using acetone, then 785 μL of acetone-DIM solution were mixed with 185.2 mg of triton X-100 prior the addition of 42 μL of silk fibroin solution at 5% w/v. The mixture was mixed by vortex for 1 min and then centrifugated at 14,000 rpm, 30 min at 4 °C (Microfuge 22R, Beckman Coulter, CA, USA). The pellet was treated as mentioned above for the SFNP production. For its part, the supernatant was used to determine the drug loading indirectly by quantifying the nonencapsulated DIM. The supernatant was analyzed by reverse phase HPLC (Shimadzu LC-2050C, Kyoto, Japan) using a 4.5 × 250 mm, 5 μm Luna C18(2) column (Phenomenex, CA.USA). The mobile phases were water (phase A) and ACN (phase B). The gradient (A/B) was 60/40 0−5 min, 35/65 5−20 min, and 0/100 20−35 min. The samples (10 μL), diluted with methanol, were run at 1 mL min^{-1} flow rate using a column temperature of 30 °C. The DIM was detected at λ 224 nm using a UV detector. A calibration curve of DIM was performed from 1 to 150 μM. The drug loading was calculated using eq 1

$$\text{drug loading percentage } (\%) = \frac{\text{DIM}_i - \text{DIM}_f}{\text{SF}}(100) \quad (1)$$

where DIM$_i$ is the initial mass of DIM, DIM$_f$ is the mass of free DIM after the encapsulation, and SF is the mass of SFNP.

Physicochemical Characterization of SFNP. The size, PDI, and zeta potential of SFNP were determined by DLS using Zetasizer Nano ZSP (Malvern, USA). The nanoparticles were diluted in HPLC water before DLS measurements. The measurements were done by triplicate of independent synthesis experiments, and the results were expressed as average ± SE. The morphology of SFNP was observed by SEM using EVO MA 25 (Zeiss, Thornwood, NY, USA) at 20 kV and 20 000-fold magnification. ATR−FTIR was carried out using a PerkinElmer Spectrum ONE instrument (Boston, MA. US) over the wavenumber range of 600−4000 cm^{-1} with a resolution of 1 cm^{-1} and averaging eight scans per spectrum. Before FTIR analysis, the nanoparticles were lyophilized using a Freeze Plus system (LabConco, MO, USA). OriginPro 2024 software was used for peak deconvolution of the amide I region (1590−1700 cm^{-1}) to determine the secondary structure of fibroin nanoparticles. The obtained peaks were area-normalized, and the relative areas of each peak were used to determine the secondary structure composition.

Determination of Antioxidant Capacity of SFNP. The antioxidant capacity of SFNP was determined based on the discoloration of the ABTS radical cation after its reduction to ABTS following the procedure reported by Enriquez-Ochoa et al.[54] with some modifications. Briefly, a 1:1 mixture of fresh 7 mM ABTS aqueous solution and 2.45 mM potassium persulfate solution was incubated under dark conditions at 25 °C for 16−18 h before its use. Then, the mixture was diluted with ethanol to reach an absorbance of 0.700 ± 0.005 at 734 nm. The reaction mixture was done by mixing 20 μL of the sample with 80 μL of ABTS diluted solution and incubating for 7 min under dark conditions. Then, the absorbance at 734 nm was measured using a microplate reader (Synergy HT Biotek, VT, USA). A calibration curve was performed using Trolox ethanolic solution as a standard (12.5−150 μM). The inhibition percentage of the ABTS radical cations was determined using eq 2

$$\text{inbibition } (\%) = \frac{(A_{C-} - A_s)}{(A_{C-} - A_{C+})} \quad (2)$$

where A_{C-} is the absorbance of the negative control, A_{C+} is the absorbance of the positive control, and A_S is the absorbance of the sample. Negative and positive controls were water and 150 μM Trolox solution, respectively. For DIM antioxidant activity, different ethanolic DIM solutions (10−1000 μM) were prepared and assessed following the previous method. The antioxidant capacity is expressed as μM Trolox equivalents.

Cell Culture and Differentiation. The murine embryo fibroblast 3T3-L1 (ATCC CL-173) cell line was obtained from

https://doi.org/10.1021/acsomega.4c07203
ACS Omega 2024, 9, 47661−47671

the American Type Culture Collection (ATCC, Manassas, VA, USA). Cells were cultured in plastic sterile flasks (Life Technologies, NY, USA) at 37 °C under a 5% CO_2 atmosphere, using a DMEM F-12 medium (Life Technologies, Grand Island, NY, USA), supplemented with 1 μg mL^{-1} penicillin and 2.5 × 10^{-3} μg mL^{-1} streptomycin, and 10% FBS (Life Technologies, Grand Island, NY). The differentiation was done following the method of Reed & Lane with modifications.[55] For differentiation, 3T3-L1 cells were seeded at 1 × 10^5. Once attached cells to the flask, DMEM was replaced by differentiation media (DMI) that included 0.5 mM 3-isobutyl-1-methylxanthine (IBMX, I7018, Sigma-Aldrich, St. Louis, MO, USA), 0.5 μM dexamethasone (Allin, Chinoin, China), and 10 mg mL^{-1} of insulin (Humulin R; Eli Lilly) in supplemented DMEM for 3 days. After cells were switched to maintenance media (supplemented DMEM with 10 mg mL^{-1} of insulin) for 3 days, then cell media was replaced with the supplemented DMEM every day until day 10. To analyze the effect of DIM encapsulation, cells were treated with 5 or 50 μM of SFNP-DIM, DIM, or SFNP during the differentiation and maturation period until harvesting cells. The equivalent concentration of SFNP-DIM was determined based on DIM drug loading.

Cell Viability Analysis. The relative cell viability on 3T3-L1 preadipocytes and white-like adipocytes was determined by the Alamar blue viability test (Life Technologies, Carlsbad, CA). This assay measures resazurin reduction by the metabolic activity of cells to resorufin by fluorescence. In brief, 5 × 10^3 cells were seeded per well in 96-well plates, then attached cells were stimulated for 24 h with DIM, SFNP, or SFNP-DIM at different concentrations (0, 0.1, 1, 5, 50, and 100 μM). The equivalent concentration of SFNP-DIM was determined based on DIM drug loading. At the end of each stimulus, relative cell viability was determined based on untreated cells.

Oil Red Stain. Intracellular lipid droplet content was analyzed using an oil red stain following the procedure of Kaczmarek with modifications.[56] In brief, 8 × 10^4 cells were seeded per well in 12-well plates. At the end of the stimuli, cells were washed twice with PBS, then fixed with formaldehyde 10% for 15 min at room temperature. After two wash cycles, cells were stained with oil red 0.3% (w/v) at room temperature for 15 min in a shake. Finally, cells were washed with distilled water. Representative images were obtained using Zeiss-AXIO microscopy (Zeiss, Oberkochen, Germany) and the camera Zeiss-Axiocam 208 color (Zeiss, Oberkochen, Germany).

Triglyceride Quantification. Triglyceride quantification was determined using a colorimetric kit (Triglycerides-LQ, SPINREACT, Girona, Spain). In brief, 8 × 10^4 differentiated adipocytes were washed with PBS, then, were lysed by scraping using 1% triton X-100 solution. In this assay, triglycerides were hydrolyzed into glycerol and fatty acids, and finally, an oxide-reduction reaction produced a red color proportional to triglyceride content. Concentration was read on a spectrophotometer (SYNERGY HT, Biotek, Winooski, Vermont, USA) at 505 nm based on a standard sample. Also, triglyceride quantification was normalized to intracellular protein content.

Total Protein Quantification. Total protein was determined using the Lowry method. This assay is based on the reaction of Cu^+, a product obtained from the oxidation of peptide bonds, with Folin−Ciocalteu (Merk, Darmstadt, Germany) reagent. In brief, 8 × 10^4 differentiated adipocytes were washed with PBS, then, were lysed by scraping using 1% triton X-100 solution. Samples were incubated with biuret solution (4 mg mL^{-1} NaOH, 20 mg mL^{-1} Na_2CO_3, 10 mg mL^{-1} $KNaC_4H_4O_6$, and 5 mg mL^{-1} $CuSO_4$) for 10 min. Finally, samples were incubated with the Folin solution for 10 min. The quantification was done on a microplate reader (SYNERGY HT, Biotek, Winooski, Vermont, USA) at 570 nm based on a BSA standard curve.

Statistical Analysis. All data were analyzed using GraphPad Prism (GraphPad Software, San Diego, CA, USA). The results given in this study represent the mean of at least three independent experiments done in triplicate (mean ± SE). Statistical analysis was done using a paired Student's *t*-test. The statistical significance was defined as $p < 0.05$.

■ ASSOCIATED CONTENT

Supporting Information

The Supporting Information is available free of charge at https://pubs.acs.org/doi/10.1021/acsomega.4c07203.

Morphology of white-like adipocytes at 10 days of differentiation, oil red staining of white-like adipocytes at 10 days of differentiation, and triglyceride quantification of white-like adipocytes at 10 days of differentiation treated with 5 μM of DIM, SFNP, and SFNP-DIM, raw micrographs of SFNP using acetone as a solvent. Nanoparticles prepared by the reverse microemulsion method using 5% w/v of silk fibroin solution, raw micrographs of SFNP using ethanol as a solvent, nanoparticles prepared by the reverse microemulsion method using 5% w/v of silk fibroin solution, raw micrographs of SFNP loaded with DIM, and nanoparticles prepared by the reverse microemulsion method using 5% w/v of silk fibroin solution at DIM/fibroin mass ratio 1:1 (PDF)

■ AUTHOR INFORMATION

Corresponding Author

Karla Mayolo-Deloisa − *Institute for Obesity Research, Tecnologico de Monterrey, Monterrey, Nuevo León 64849, Mexico; Escuela de Ingeniería y Ciencias, Centro de Biotecnología-FEMSA, Tecnologico de Monterrey, Monterrey, Nuevo León 64849, Mexico;* orcid.org/0000-0002-2826-2518; Email: kmayolo@tec.mx

Authors

Calef Sánchez-Trasviña − *Institute for Obesity Research, Tecnologico de Monterrey, Monterrey, Nuevo León 64849, Mexico; Escuela de Ingeniería y Ciencias, Centro de Biotecnología-FEMSA, Tecnologico de Monterrey, Monterrey, Nuevo León 64849, Mexico*

Helen Y. Lorenzo-Anota − *Institute for Obesity Research, Tecnologico de Monterrey, Monterrey, Nuevo León 64849, Mexico; Escuela de Medicina y Ciencias de la Salud, Tecnológico de Monterrey, Monterrey, Nuevo León 64849, Mexico*

Aleyda M. Escobar-Fernández − *Institute for Obesity Research, Tecnologico de Monterrey, Monterrey, Nuevo León 64849, Mexico; Escuela de Ingeniería y Ciencias, Centro de Biotecnología-FEMSA, Tecnologico de Monterrey, Monterrey, Nuevo León 64849, Mexico*

David Lezama-Aguilar − *Institute for Obesity Research, Tecnologico de Monterrey, Monterrey, Nuevo León 64849, Mexico; Escuela de Ingeniería y Ciencias, Centro de*

https://doi.org/10.1021/acsomega.4c07203
ACS Omega 2024, 9, 47661−47671

Biotecnología-FEMSA, Tecnologico de Monterrey, Monterrey, Nuevo León 64849, Mexico

Adriana Morales-Martínez − *Institute for Obesity Research, Tecnologico de Monterrey, Monterrey, Nuevo León 64849, Mexico; Escuela de Medicina y Ciencias de la Salud, Tecnológico de Monterrey, Monterrey, Nuevo León 64849, Mexico*

Ana Vélez-Barceló − *Escuela de Ingeniería y Ciencias, Centro de Biotecnología-FEMSA, Tecnologico de Monterrey, Monterrey, Nuevo León 64849, Mexico*

Jorge Benavides − *Institute for Obesity Research, Tecnologico de Monterrey, Monterrey, Nuevo León 64849, Mexico; Escuela de Ingeniería y Ciencias, Centro de Biotecnología-FEMSA, Tecnologico de Monterrey, Monterrey, Nuevo León 64849, Mexico*

Omar Lozano − *Institute for Obesity Research, Tecnologico de Monterrey, Monterrey, Nuevo León 64849, Mexico; Escuela de Medicina y Ciencias de la Salud, Tecnológico de Monterrey, Monterrey, Nuevo León 64849, Mexico*

Marco Rito-Palomares − *Institute for Obesity Research, Tecnologico de Monterrey, Monterrey, Nuevo León 64849, Mexico; Escuela de Medicina y Ciencias de la Salud, Tecnológico de Monterrey, Monterrey, Nuevo León 64849, Mexico*

Complete contact information is available at: https://pubs.acs.org/10.1021/acsomega.4c07203

Author Contributions

The manuscript was written through contributions of all authors. All authors have given approval to the final version of the manuscript.

Notes

The authors declare no competing financial interest.

■ ACKNOWLEDGMENTS

The authors would like to thank the financial support from Tecnologico de Monterrey through the "Challenge-Based Research Funding Program 2022" (Project ID IJXT070-22EG57001) and to Regina E. Vargas-Mejia and Angel H. Cabrera-Ramirez to their support to carry out the SEM and ATR−FTIR experiments, respectively.

■ REFERENCES

(1) Chakhtoura, M.; Haber, R.; Ghezzawi, M.; Rhayem, C.; Tcheroyan, R.; Mantzoros, C. S. Pharmacotherapy of Obesity: An Update on the Available Medications and Drugs under Investigation. *EClinicalMedicine* **2023**, *58*, 101882.

(2) Chang, Y. H.; Hung, H. Y. Recent Advances in Natural Anti-Obesity Compounds and Derivatives Based on in Vivo Evidence: A Mini-Review. *Eur. J. Med. Chem.* **2022**, *237*, 114405.

(3) World Obesity Federation, World Obesity Atlas 2023. 2023, https://data.worldobesity.org/publications/?cat=19 (accessed May 5, 2024).

(4) Verduci, E.; Di Profio, E.; Fiore, G.; Zuccotti, G. Integrated Approaches to Combatting Childhood Obesity. *Ann. Nutr. Metab.* **2022**, *78*, 8−19.

(5) Lustig, R. H.; Collier, D.; Kassotis, C.; Roepke, T. A.; Kim, M. J.; Blanc, E.; Barouki, R.; Bansal, A.; Cave, M. C.; Chatterjee, S.; Choudhury, M.; Gilbertson, M.; Lagadic-Gossmann, D.; Howard, S.; Lind, L.; Tomlinson, C. R.; Vondracek, J.; Heindel, J. J. Obesity I: Overview and Molecular and Biochemical Mechanisms. *Biochem. Pharmacol.* **2022**, *199*, 115012.

(6) Fontaine, K. R.; Redden, D. T.; Wang, C.; Westfall, A. O.; Allison, D. B. Years of Life Lost Due to Obesity. *JAMA* **2003**, *289*, 187−193.

(7) Wen, X.; Zhang, B.; Wu, B.; Xiao, H.; Li, Z.; Li, R.; Xu, X.; Li, T. Signaling Pathways in Obesity: Mechanisms and Therapeutic Interventions. *Signal Transduction Targeted Ther.* **2022**, *7*, 298.

(8) Abbasi, M.; Fan, Z.; Dawson, J. A.; Wang, S. Transdermal Delivery of Metformin Using Dissolving Microneedles and Iontophoresis Patches for Browning Subcutaneous Adipose Tissue. *Pharmaceutics* **2022**, *14*, 879.

(9) Müller, T. D.; Blüher, M.; Tschöp, M. H.; DiMarchi, R. D. Anti-Obesity Drug Discovery: Advances and Challenges. *Nat. Rev. Drug Discovery* **2022**, *21*, 201−223.

(10) Shende, P.; Narvenker, R. Herbal Nanotherapy: A New Paradigm over Conventional Obesity Treatment. *J. Drug Delivery Sci. Technol.* **2021**, *61*, 102291.

(11) Carrasco-Pozo, C.; Cires, M. J.; Gotteland, M. Quercetin and Epigallocatechin Gallate in the Prevention and Treatment of Obesity: From Molecular to Clinical Studies. *J. Med. Food* **2019**, *22*, 753−770.

(12) Zhao, J.; Luo, D.; Zhang, Z.; Fan, N.; Wang, Y.; Nie, H.; Rong, J. Celastrol-Loaded PEG-PCL Nanomicelles Ameliorate Inflammation, Lipid Accumulation, Insulin Resistance and Gastrointestinal Injury in Diet-Induced Obese Mice. *J. Controlled Release* **2019**, *310*, 188−197.

(13) Yang, H.; Seo, S. G.; Shin, S. H.; Min, S.; Kang, M. J.; Yoo, R.; Kwon, J. Y.; Yue, S.; Kim, K. H.; Cheng, J. X.; Kim, J. R.; Park, J. S.; Kim, J. H.; Park, J. H. Y.; Lee, H. J.; Lee, K. W. 3,3′-Diindolylmethane Suppresses High-Fat Diet-Induced Obesity through Inhibiting Adipogenesis of Pre-Adipocytes by Targeting USP2 Activity. *Mol. Nutr. Food Res.* **2017**, *61*, 1700119.

(14) Mattiazzi, J.; Marcondes Sari, M. H.; Brum, T. d. B.; Araújo, P. C. O.; Nadal, J. M.; Farago, P. V.; Nogueira, C. W.; Cruz, L. 3,3′-Diindolylmethane Nanoencapsulation Improves Its Antinociceptive Action: Physicochemical and Behavioral Studies. *Colloids Surf., B* **2019**, *181*, 295−304.

(15) Mattiazzi, J.; Sari, M. H. M.; Lautenchleger, R.; Dal Prá, M.; Braganhol, E.; Cruz, L. Incorporation of 3,3′-Diindolylmethane into Nanocapsules Improves Its Photostability, Radical Scavenging Capacity, and Cytotoxicity Against Glioma Cells. *AAPS PharmSciTech* **2019**, *20*, 49.

(16) Choi, K. M.; Yoo, H. S. 3,3′-Diindolylmethane Enhances Glucose Uptake Through Activation of Insulin Signaling in 3T3-L1 Adipocytes. *Obesity* **2018**, *26*, 1153−1160.

(17) Khan, A.; Wang, C.; Sun, X.; Killpartrick, A.; Guo, M. Preparation and Characterization of Whey Protein Isolate−Dim Nanoparticles. *Int. J. Mol. Sci.* **2019**, *20*, 3917.

(18) Godugu, C.; Doddapaneni, R.; Safe, S. H.; Singh, M. Novel Diindolylmethane Derivatives Based NLC Formulations to Improve the Oral Bioavailability and Anticancer Effects in Triple Negative Breast Cancer. *Eur. J. Pharm. Biopharm.* **2016**, *108*, 168−179.

(19) Ash, G. I.; Kim, D.; Choudhury, M. Promises of Nano-therapeutics in Obesity. *Trends Endocrinol. Metab.* **2019**, *30*, 369−383.

(20) Ferrer-Tasies, L.; Santana, H.; Cabrera-Puig, I.; González-Mira, E.; Ballell-Hosa, L.; Castellar-Álvarez, C.; Córdoba, A.; Merlo-Mas, J.; Gerónimo, H.; Chinea, G.; Falcón, V.; Moreno-Calvo, E.; Pedersen, J. S.; Romero, J.; Navarro-Requena, C.; Valdés, C.; Limonta, M.; Berlanga, J.; Sala, S.; Martínez, E.; Veciana, J.; Ventosa, N. Recombinant Human Epidermal Growth Factor/Quatsome Nanoconjugates: A Robust Topical Delivery System for Complex Wound Healing. *Adv. Ther.* **2021**, *4*, 2000260.

(21) Anselmo, A. C.; Mitragotri, S. Nanoparticles in the Clinic: An Update. *Bioeng. Transl. Med.* **2019**, *4*, No. e10143.

(22) Luo, Y.; Wang, T. T. Y.; Teng, Z.; Chen, P.; Sun, J.; Wang, Q. Encapsulation of Indole-3-Carbinol and 3,3′-Diindolylmethane in Zein/Carboxymethyl Chitosan Nanoparticles with Controlled Release Property and Improved Stability. *Food Chem.* **2013**, *139*, 224−230.

(23) Pham, D. T.; Tiyaboonchai, W. Fibroin Nanoparticles: A Promising Drug Delivery System. *Drug Delivery* **2020**, *27*, 431−448.

(24) Zhang, H.; Xu, D.; Zhang, Y.; Li, M.; Chai, R. Silk Fibroin Hydrogels for Biomedical Applications. *Smart Med.* **2022**, *1*, No. e20220011.
(25) Zhang, Y. Q.; De Shen, W.; Xiang, R. L.; Zhuge, L. J.; Gao, W. J.; Wang, W. B. Formation of Silk Fibroin Nanoparticles in Water-Miscible Organic Solvent and Their Characterization. *J. Nanopart. Res.* **2007**, *9*, 885−900.
(26) Mocchi, M.; Bari, E. Silk-Fibroin Nano-Drug Delivery Systems. In *Silk-based Drug Delivery Systems*; Bari, E., Perteghella, S., Torre, M. L., Eds.; The Royal Society of Chemistry, 2020; pp 88−119.
(27) Rajendra, P. K. M.; Nidamanuri, B. S. S.; Balan, A. P.; Venkatachalam, S.; Jawahar, N. A Review on Structure, Preparation and Applications of Silk Fibroin-Based Nano-Drug Delivery Systems. *J. Nanopart. Res.* **2022**, *24*, 141.
(28) Myung, S. J.; Kim, H. S.; Kim, Y.; Chen, P.; Jin, H. J. Fluorescent Silk Fibroin Nanoparticles Prepared Using a Reverse Microemulsion. *Macromol. Res.* **2008**, *16*, 604−608.
(29) Joye, I. J.; McClements, D. J. Production of Nanoparticles by Anti-Solvent Precipitation for Use in Food Systems. *Trends Food Sci. Technol.* **2013**, *34*, 109−123.
(30) Thanh, N. T. K.; Maclean, N.; Mahiddine, S. Mechanisms of Nucleation and Growth of Nanoparticles in Solution. *Chem. Rev.* **2014**, *114*, 7610−7630.
(31) Lammel, A. S.; Hu, X.; Park, S. H.; Kaplan, D. L.; Scheibel, T. R. Controlling Silk Fibroin Particle Features for Drug Delivery. *Biomaterials* **2010**, *31*, 4583−4591.
(32) Lin, L.; Luo, C.; Li, C.; Abdel-Samie, M. A.; Cui, H. Eugenol/Silk Fibroin Nanoparticles Embedded Lycium Barbarum Polysaccharide Nanofibers for Active Food Packaging. *Food Packag. Shelf Life* **2022**, *32*, 100841.
(33) Mudhol, S.; Serva Peddha, M. Development of Capsaicin Loaded Nanoparticles Based Microneedle Patch for Transdermal Drug Delivery. *J. Drug Delivery Sci. Technol.* **2023**, *80*, 104120.
(34) Seib, F. P.; Jones, G. T.; Rnjak-Kovacina, J.; Lin, Y.; Kaplan, D. L. PH-Dependent Anticancer Drug Release from Silk Nanoparticles. *Adv. Healthcare Mater.* **2013**, *2*, 1606−1611.
(35) Zeng, S.; Tang, Q.; Jiang, K.; Tang, X. Fabrication of Metformin and Survivin SiRNA Encapsulated into Polyethyleneimine-Altered Silk Fibroin Nanoparticles for the Treatment of Nasopharyngeal Carcinoma. *Process Biochem.* **2023**, *125*, 36−46.
(36) Kundu, J.; Chung, Y.-I.; Kim, Y. H.; Tae, G.; Kundu, S. C. Silk Fibroin Nanoparticles for Cellular Uptake and Control Release. *Int. J. Pharm.* **2010**, *388*, 242−250.
(37) Stuart, B. Biological Applications. In *Infrared Spectroscopy: Fundamentals and Applications; Analytical Techniques in the Sciences*; Ando, D. J., Stuart, B. H., Eds.; John Wiley & Sons, Ltd, 2004; pp 137−165.
(38) Ding, B.; Wahid, M. A.; Wang, Z.; Xie, C.; Thakkar, A.; Prabhu, S.; Wang, J. Triptolide and Celastrol Loaded Silk Fibroin Nanoparticles Show Synergistic Effect against Human Pancreatic Cancer Cells. *Nanoscale* **2017**, *9*, 11739−11753.
(39) Solomun, J. I.; Totten, J. D.; Wongpinyochit, T.; Florence, A. J.; Seib, F. P. Manual Versus Microfluidic-Assisted Nanoparticle Manufacture: Impact of Silk Fibroin Stock on Nanoparticle Characteristics. *ACS Biomater. Sci. Eng.* **2020**, *6*, 2796−2804.
(40) Boakye, C. H. A.; Patel, K.; Doddapaneni, R.; Bagde, A.; Behl, G.; Chowdhury, N.; Safe, S.; Singh, M. Ultra-Flexible Nanocarriers for Enhanced Topical Delivery of a Highly Lipophilic Antioxidative Molecule for Skin Cancer Chemoprevention. *Colloids Surf., B* **2016**, *143*, 156−167.
(41) Wang, C.; Zhou, X.; Wang, H.; Sun, X.; Guo, M. Interactions between β-Lactoglobulin and 3,3′-Diindolylmethane in Model System. *Molecules* **2019**, *24*, 2151.
(42) Totten, J. D.; Wongpinyochit, T.; Carrola, J.; Duarte, I. F.; Seib, F. P. PEGylation-Dependent Metabolic Rewiring of Macrophages with Silk Fibroin Nanoparticles. *ACS Appl. Mater. Interfaces* **2019**, *11*, 14515−14525.
(43) Wongkrongsak, S.; Tangthong, T.; Pasanphan, W. Electron Beam Induced Water-Soluble Silk Fibroin Nanoparticles as a Natural Antioxidant and Reducing Agent for a Green Synthesis of Gold Nanocolloid. *Radiat. Phys. Chem.* **2016**, *118*, 27−34.
(44) Pham, D. T.; Saelim, N.; Cornu, R.; Béduneau, A.; Tiyaboonchai, W. Crosslinked Fibroin Nanoparticles: Investigations on Biostability, Cytotoxicity, and Cellular Internalization. *Pharmaceuticals* **2020**, *13*, 86.
(45) Naserzadeh, P.; Mortazavi, S. A.; Ashtari, K.; Seydi, E.; Pourahmad, J. Evaluation of the Toxicity Effects of Silk Fibroin on Isolated Fibroblast and Huvec Cells. Iran. *J. Pharm. Res.* **2018**, *17*, 134−145.
(46) Chon, J.; Lee, K.; Park, Y.; Park, K.; Yeo, J. Anti-Adipogenic Effect of Hydrolysate Silk Fibroin in 3T3-L1 Cells. *Int. J. Indust. Entomol. Biomater.* **2010**, *21*, 169−174.
(47) Ghaben, A. L.; Scherer, P. E. Adipogenesis and Metabolic Health. *Nat. Rev. Mol. Cell Biol.* **2019**, *20*, 242−258.
(48) Nunn, E. R.; Shinde, A. B.; Zaganjor, E. Weighing in on Adipogenesis. *Front. Physiol.* **2022**, *13*, 821278.
(49) Zebisch, K.; Voigt, V.; Wabitsch, M.; Brandsch, M. Protocol for Effective Differentiation of 3T3-L1 Cells to Adipocytes. *Anal. Biochem.* **2012**, *425*, 88−90.
(50) Jakab, J.; Miškić, B.; Mikšić, S.; Juranić, B.; Ćosić, V.; Schwarz, D.; Včev, A. Adipogenesis as a Potential Anti-Obesity Target: A Review of Pharmacological Treatment and Natural Products. *Diabetes, Metab. Syndr. Obes.: Targets Ther.* **2021**, *14*, 67−83.
(51) Grabner, G. F.; Xie, H.; Schweiger, M.; Zechner, R. Lipolysis Cellular Mechanisms for Lipid Mobilization from Fat Stores. *Nat. Metab.* **2021**, *3*, 1445−1465.
(52) Lee, J.; Yue, Y.; Park, Y.; Lee, S.-H. 3,3′-Diindolylmethane Suppresses Adipogenesis Using AMPKα-Dependent Mechanism in 3T3-L1 Adipocytes and Caenorhabditis elegans. *J. Med. Food* **2017**, *20*, 646−652.
(53) Lee, K.; Jin, H.; Chei, S.; Lee, J.-Y.; Oh, H.-J.; Lee, B.-Y. Dietary Silk Peptide Prevents High-Fat Diet-Induced Obesity and Promotes Adipose Browning by Activating AMP-Activated Protein Kinase in Mice. *Nutrients* **2020**, *12*, 201.
(54) Enriquez-Ochoa, D.; Sánchez-Trasviña, C.; Hernández-Sedas, B.; Mayolo-Deloisa, K.; Zavala, J.; Rito-Palomares, M.; Valdez-García, J. E. Aqueous Two-Phase Extraction of Phenolic Compounds from Sedum Dendroideum with Antioxidant Activity and Anti-Proliferative Properties against Breast Cancer Cells. *Sep. Purif. Technol.* **2020**, *251*, 117341.
(55) Reed, B. C.; Lane, M. D. Insulin Receptor Synthesis and Turnover in Differentiating 3T3-L1 Preadipocytes. *Proc. Natl. Acad. Sci. U.S.A.* **1980**, *77* (1), 285−289.
(56) Kaczmarek, I.; Suchý, T.; Strnadová, M.; Thor, D. Qualitative and Quantitative Analysis of Lipid Droplets in Mature 3T3-L1 Adipocytes Using Oil Red O. *STAR Protoc.* **2024**, *5* (2), 102977.

https://doi.org/10.1021/acsomega.4c07203
ACS Omega 2024, 9, 47661−47671